Available online at www.sciencedirect.com

SciVerse ScienceDirect

Russian Geology and Geophysics 53 (2012) 293–306

RUSSIAN GEOLOGY AND GEOPHYSICS

www.elsevier.com/locate/rgg

Crust structure and composition in the southern Siberian craton (influence zone of Baikal rifting), from magnetotelluric data

M.I. Epov, E.V. Pospeeva *, L.V. Vitte

A.A. Trofimuk Institute of Petroleum Geology and Geophysics, Siberian Branch of the Russian Academy of Sciences, pr. Akademika Koptyuga 3, Novosibirsk, 630090, Russia

Received 13 August 2010; received in revised form 14 June 2011, accepted 15 July 2011

Abstract

The magnetotelluric (MT) profile traverses the southeastern edge of the Siberian craton and the adjacent Paleozoic Olkhon collision zone, both being within the influence area of the Baikal rifting. The processed MT data have been integrated with data on the crust structure and composition, as well as with magnetic, gravity, and seismic patterns. Large resistivity lows are interpreted with reference to new geothermal models of rifted crust in the Baikal region. The northwestern and southeastern flanks of the profile corresponding, respectively, to the craton and the collision zone differ markedly in the crust structure and composition and in the intensity of rifting-related processes, the difference showing up in the resistivity pattern. The high-grade metamorphic and granitic crust of the craton basement in the northwestern profile flank is highly resistive but it includes a conductor (less than 50 ohm · m) below 16–20 km and a nearly vertical conductive layer in the upper crust. The crust in the southeastern part, within the collision zone, is lithologically heterogeneous and heavily faulted. High resistivities are measured mainly in the upper crust composed of collisional plutonic and metamorphic complexes. Large and deep resistivity lows over the greatest part of the section are due to Cenozoic activity and rift-related transcrustal faults that vent mantle fluids constantly recharged from deeper mantle.

Keywords: magnetotelluric (MT) soundings; resistivity; rift-related faults; collision zone; igneous and metamorphic rocks

Introduction

Magnetotelluric surveys in the Baikal area were initiated in the mid-1960s by V.I. Pospeyev, V.I. Mikhalevsky, and V.P. Gornostaev. V.I. Pospeyev was the first to prove the existence of a conductive layer in the crust (Pospeyev, 1976; Pospeyev et al., 1989). Crustal conductors of that kind were reported also later from Baikal rift and elsewhere (Adam, 1976; Berdichevsky et al., 1999; Popov, 1990). One possible explanation of locally conductive crust is water fluids generated out of hydrogen rising from the mantle (Letnikov et al., 1977).

The MT data collected in the 1960s through 1970s revealed three major resistivity zones in the southern Siberian craton: the craton proper, the Baikal fold area, and a transition between them. The contrasting resistivity patterns in the craton and in the rift were attributed to difference in the lithospheric thermal regimes (Gornostaev, 1967, 1979; Gornostaev et al., 1970; Pospeyev, 1976; Pospeyev et al., 1989).

Later Popov (1990) suggested a 3D model of the Baikal area based on synthesized MT data which imaged a prominent conductor in the crust beneath the Baikal rift, with a resistivity from 100 to 40 ohm · m, and a mantle conductor corresponding to the asthenosphere about 100 km below the surface.

The cited studies have contributed a lot to the knowledge of the subsurface in the area but were spatially limited and could not provide a large-scale coverage.

In 2009 a team from the Trofimuk Institute of Petroleum Geology and Geophysics (Novosibirsk) began MT surveys on long transects in order to investigate the resistivity structure of the stable Siberian craton, the transition zone, and the Baikal rift. Currently two profiles have been collected, one (I–I) from Bayandai Village to Krestovskii Cape on the western side of Lake Baikal and the other (II–II) within the Olkhon collision zone (Fig. 1). The MT data acquired with digital instruments and processed using advanced techniques have furnished new evidence of the regional resistivity patterns and thus extended and specified the previous results. The

* Corresponding author.
E-mail address: pospeevaev@ipgg.nsc.ru (E.V. Pospeeva)

1068-7971/$ - see front matter
doi:10.1016/j.rgg.2012.02.006

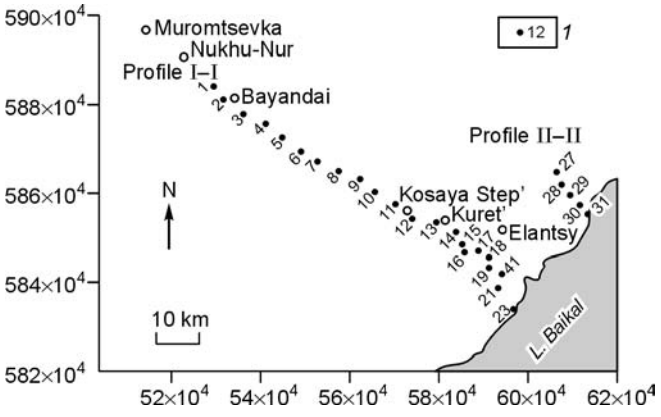

Fig. 1. Location map of MT profiles I–I and II–II. *1*, MT stations.

suggested resistivity model of the crust includes two structurally and compositionally different units in the northwestern and southeastern parts of the region, where rifting-related processes act in different ways (Pospeyev, 1976; Pospeyev et al., 1989).

Methods of MT data acquisition and processing

Magnetotelluric soundings at periods from 0.003 to 10,000 s were performed with the MTU V5 System 2000 manufactured by *Phoenix Geophysics* Ltd. (Canada). The telluric components were measured by a 2D array with 100 m long receivers, at the recording time 19–22 h. The geographic coordinates and elevations of the MT sites were positioned using GPS. Altogether MT data were acquired at twenty two sites spaced at 5 km along I–I and six sites at every 3 km along II–II.

The field data were processed with the *Phoenix Geophysics* software in which the time series of all MT components were correlated with one another, then Fourier transformed into the frequency domain, and then converted into the impedance tensor components.

Data processing and interpretation

MT data processing and interpretation aim at estimating the conductivity in the crust (sediments and bedrock) and upper mantle and creating a parametric geoelectric model. Modeling includes qualitative work of choosing the resistivity model of the area and estimating its parameters quantitatively. The qualitative interpretation of the collected MT responses is especially difficult as the resistivity structure depends on all elements of the explored medium. It is important at this stage to provide the appropriate choice of the model (Berdichevsky et al., 1997) on the basis of amplitude and phase responses, magnetotelluric (MT) and magnetovariation (MV) curves, MT polar diagrams of the impedance tensor elements, as well as computed and normalized longitudinal (profile-parallel, $\rho^{\parallel}$) and transverse (profile-orthogonal, $\rho^{\perp}$) curves of apparent resistivity (ρ_a).

Profile I–I traverses the southeastern Irkutsk amphitheater from the Lake Baikal shore across the rift strike (Fig. 1). The frequency-domain MT and MV tensors ($|Z|$ and $|W|$, respectively) found as

$$|Z| = \begin{vmatrix} Z_{xx} & Z_{xy} \\ Z_{yx} & Z_{yy} \end{vmatrix}, \quad |W| = \begin{vmatrix} W_{zx} & W_{zy} \end{vmatrix} \tag{1}$$

record the lateral heterogeneity of the subsurface and allow one to identify high- and low-resistivity zones and to estimate their size and orientation. It is important to apply formalized MT and MV tests, namely

$$N = \left| \left(1 - 4 \frac{Z_{xx} Z_{yy} - Z_{xy} Z_{yx}}{(Z_{xy} - Z_{yx})^2} \right)^{1/2} \right|, \tag{2}$$

$$skew_S = \left| \frac{Z_{xx} + Z_{xy}}{Z_{xy} - Z_{yx}} \right|, \tag{3}$$

$$skew_B = \frac{\sqrt{0.5|\mathrm{Im}\,(Z_{xy} Z_{yy}^* + Z_{xx} Z_{yx}^*)|}}{\left| Z_{xy} - Z_{yx} \right|}, \tag{4}$$

where * denotes a complex conjugate.

$$N_{mv} = ||W|| = \sqrt{|W_{zx}|^2 + |W_{zy}|^2}. \tag{5}$$

The invariant dimensionality parameters N, $skew_S$, $skew_B$, and N_{mv} (N is the magnetotelluric heterogeneity parameter, $skew_S$ is the Swift (1967) skew, $skew_B$ is the Bahr skew, and N_{mv} is the magnetovariation heterogeneity parameter) are estimated relative to the threshold δ corresponding to the instrumental error. The δ values are commonly chosen to be 0.05–0.15 in the MT test and 0.03–0.05 in the MV test (Berdichevsky and Dmitriev, 2009).

The northwestern profile flank covers the southeastern periphery of the Siberian craton exposed to rifting influence (MT sites 1–12). The sedimentary upper section has low N (<0.15) at short periods ($T \ll 1$ s) which, according to Bahr (1988), indicates that the structure is one-dimensional. The heterogeneity N grows to 0.2–0.3 at T = 1 s and as high as 0.7–0.9 at long periods of $T \gg 100$ s (Fig. 2, *a*, *b*, *c*). When the heterogeneity N is high, the skew parameters are high as well: $skew_S$ = 0.4–0.7 and $skew_B$ (> 0.3). At station 3, the heterogeneity and Swift skew are notably above the threshold over the entire bandwidth, while $skew_B$ is only 0.08 thus implying a 2D (or 3D) structure of the upper crust. The same holds for stations 6 through 12 where N and $skew_S$ reach 0.8 and 0.7, respectively, and $skew_B$ is within 0.1–0.08 (Fig. 2, *a*, *b*, *c*). In the southeastern profile part, N and $skew_S$ are the highest and $skew_B$ is the lowest in the area at short periods: N = 0.7–0.8; $skew_S$ = 0.9; $skew_B$ < 0.08 (Fig. 2, *a*, *b*, *c*), but all parameters are within the δ = 0.05–0.15 limit at $T \ll 1$ s.

Thus, the northwestern flank of the profile is a regional-scale 2D structure with localized 2D and 3D heterogeneities in the sediment cover and in the upper-middle crust; the southeastern profile flank is a local 3D feature on a 3D axisymmetrical background, except for the 1D uppermost section. This inference is consistent with the MT polar

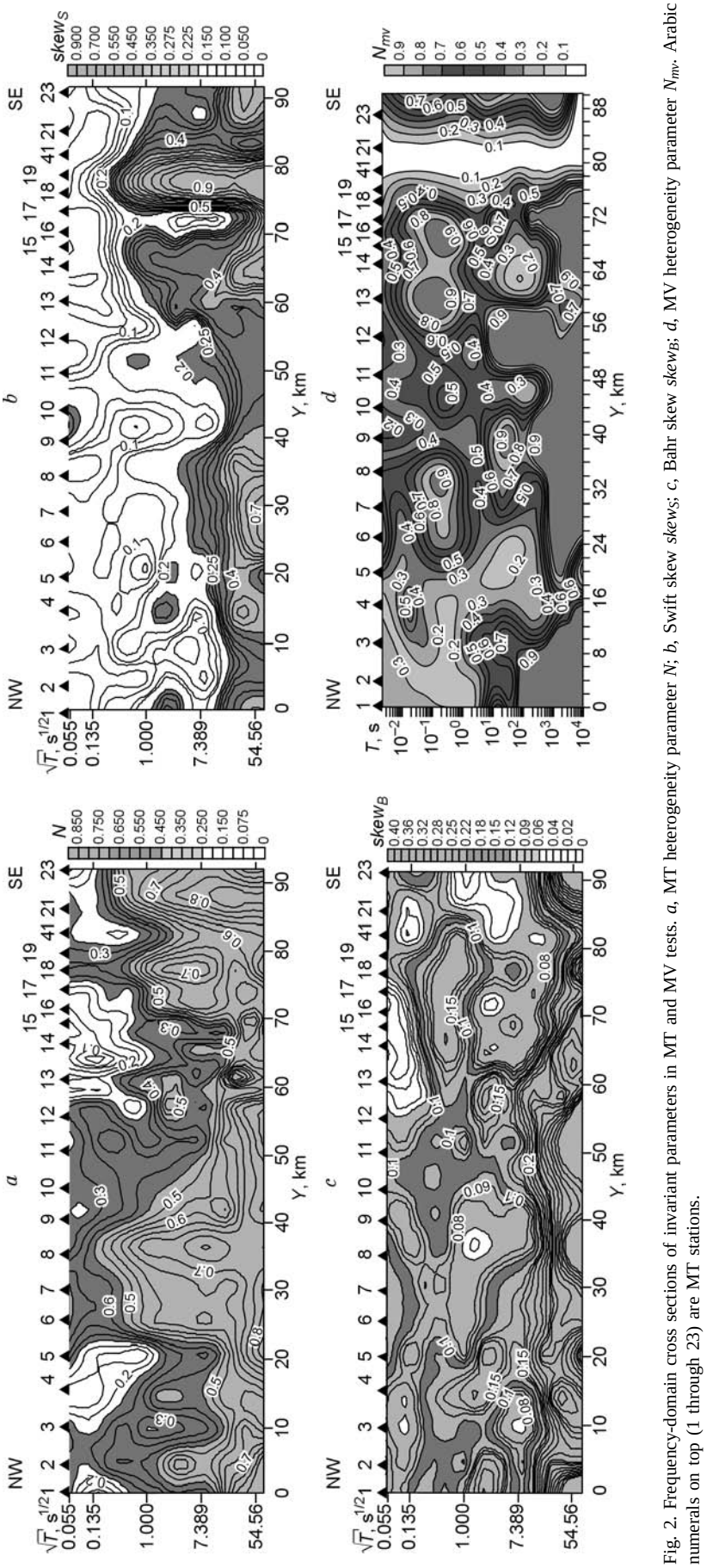

Fig. 2. Frequency-domain cross sections of invariant parameters in MT and MV tests. *a*, MT heterogeneity parameter *N*; *b*, Swift skew *skew*$_S$; *c*, Bahr skew *skew*$_B$; *d*, MV heterogeneity parameter N_{mv}. Arabic numerals on top (1 through 23) are MT stations.

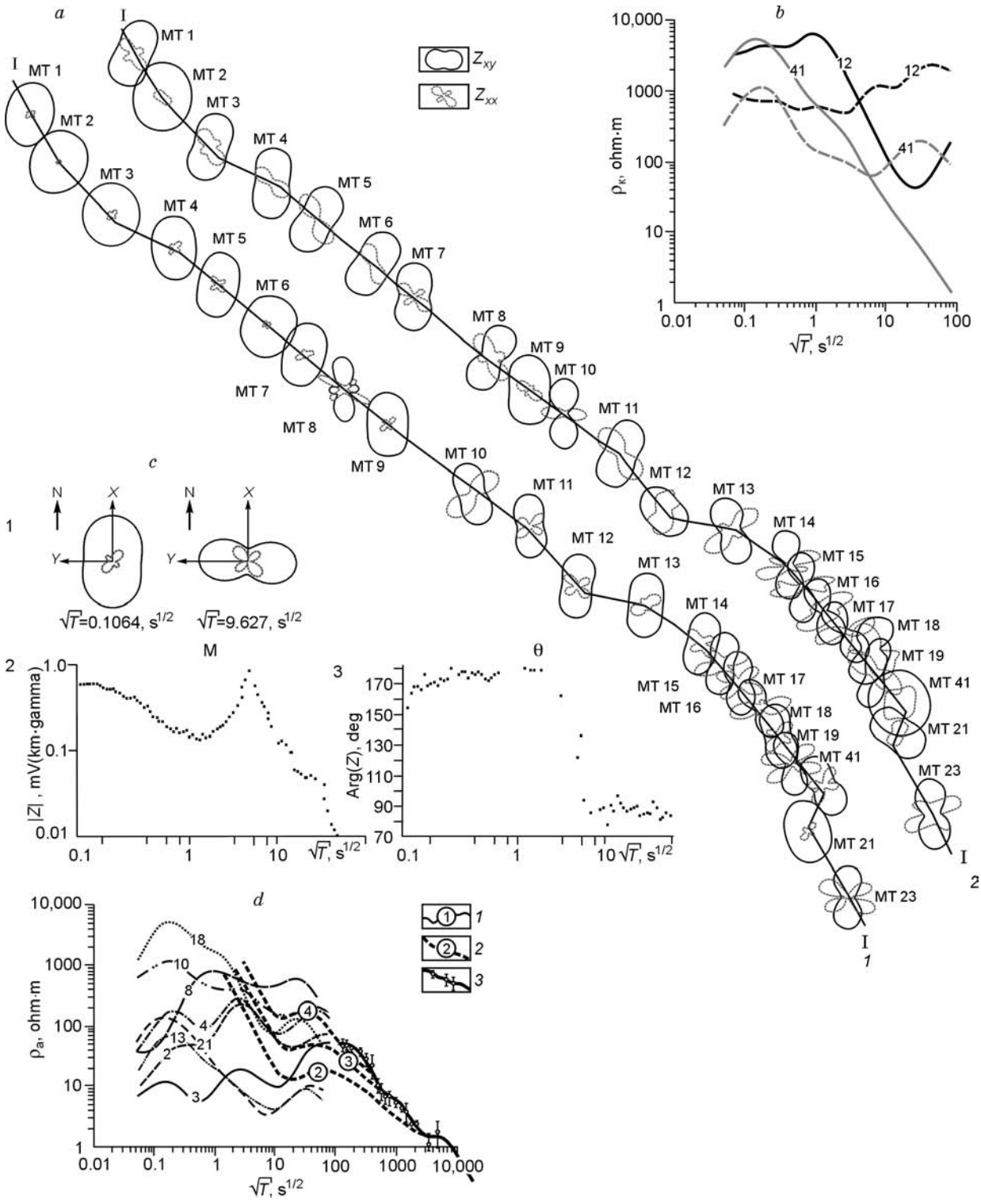

Fig. 3. Analysis of MT data collected along profile I–I. *a*, MT polar diagrams (Z_{xy}, Z_{xx}) of impedance tensor $|Z|$ at frequencies 0.04 (*1*) and 100 (*2*) Hz; *b*, longitudinal and transverse apparent resistivity curves at the strike change point; *c*, MT station 12: 1, MT polar diagrams of impedance tensor $|Z|$; 2, $M = f(\sqrt{T})$ plot; 3, $\Theta = f(\sqrt{T})$ plot; *d*, typical longitudinal MT curves: *1*, measured curves; *2*, computed curves for *PT* conditions (in circles) of rifts (2), rift margins and central parts of basins (3), basin sides (4); *3*, global MV curve.

diagrams of impedance tensor (Fig. 3, *a*), their configuration being a reliable dimensionality indicator (Berdichevsky and Dmitriev, 2009). The polar diagrams for the craton portion of the profile (Fig. 3, *a*) fit a 2D model: the $|Z_{xy}|$ diagrams are regular ovals while $|Z_{xx}|$ look like a flower with four identical petals (except for those at sites 8, 10, and 11). The diagrams for the Olkhon collision zone fit an axisymmetrical 3D model and look like those of 2D impedance.

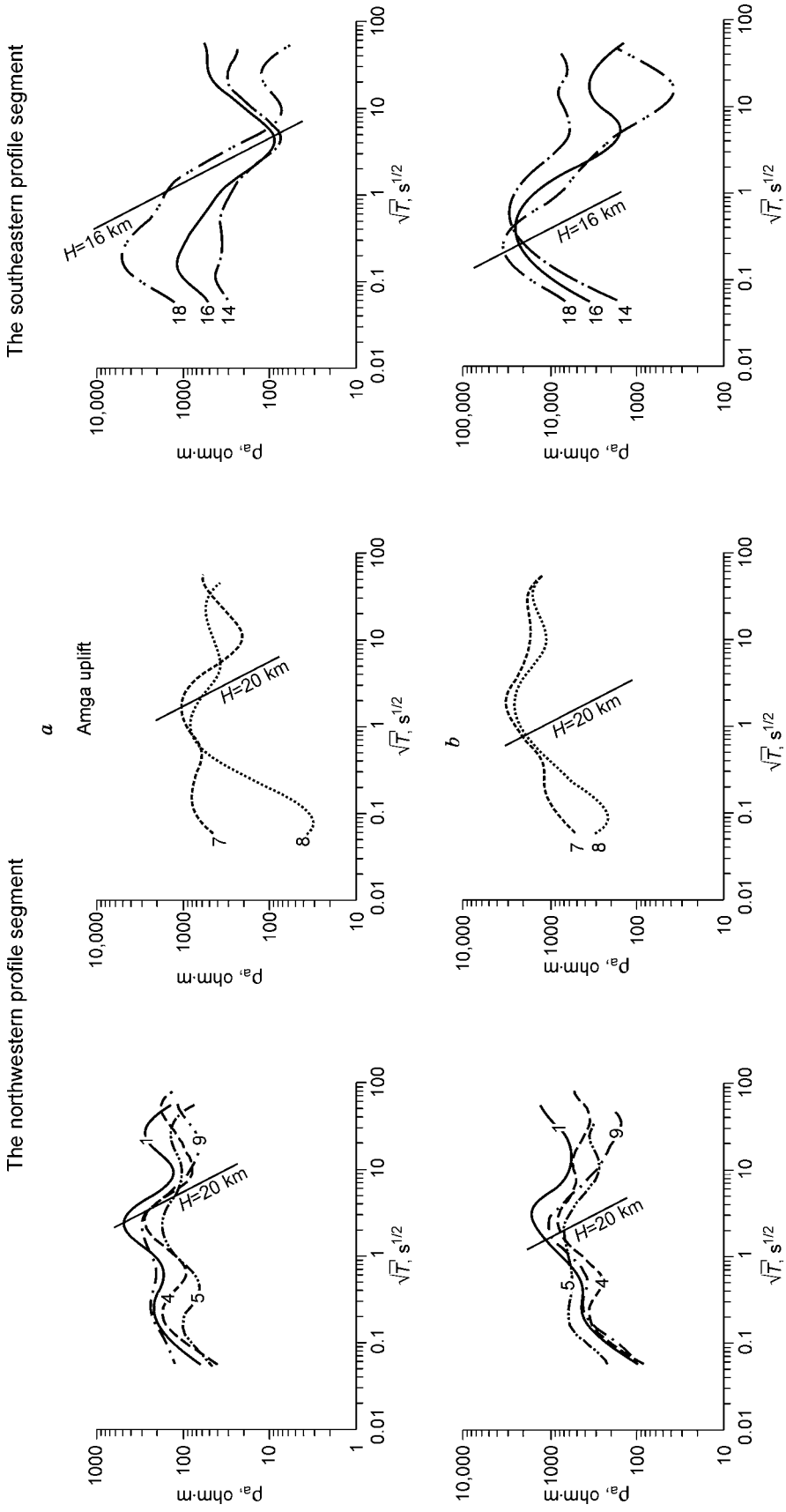

Fig. 4. Longitudinal (*a*) and transverse (*b*) apparent resistivity curves typical of northwestern and southeastern flanks of profile II. Numerals are MT stations.

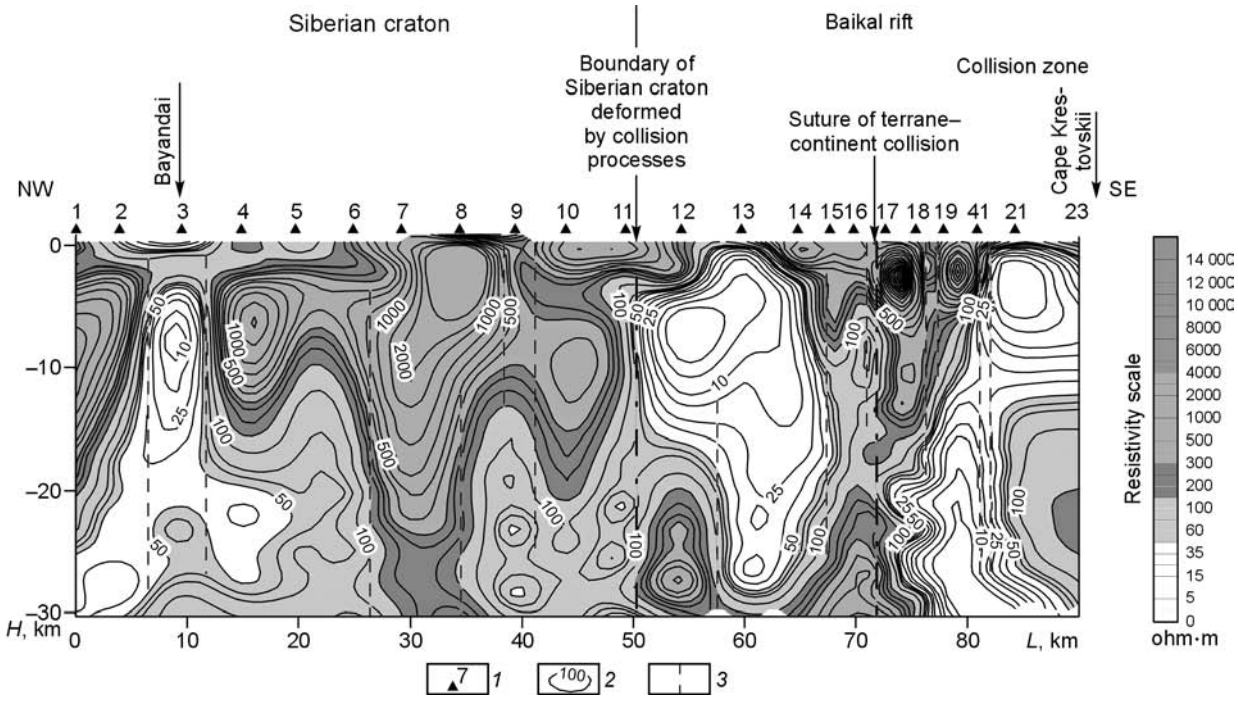

Fig. 5. Resistivity structure of lower and middle crust along profile I–I. *1*, MT stations; *2*, resistivity contour lines (ohm · m); *3*, zones of resistivity gradients (large faults).

The MT polar diagrams of stations 12 and 41 are worth of special note. The two sites are located within conductive zones associated with a system of crossing NE and W–E faults, where the model changes its strike at T = 25 and 36 s (at sites 12 and 41, respectively) and the $\rho^{\parallel}$ and $\rho^{\perp}$ curves intersect (Fig. 3, *b*). It means that the apparent resistivity curves (ρ_a) are parallel to the anomaly strike till these periods and then become orthogonal to it. Thus, the structure is no longer 1D, and one has to switch over the Z_{xy}, Z_{yx}, and $\varphi_{xy}\varphi_{yx}$ branches before computing the ρ_a curves. The strike change of the principal impedance components is prominent in the $M = f(\sqrt{T})$ and $\Theta = f(\sqrt{T})$ plots where M is the $|Z_{yx}|$ to $|Z_{xy}|$ impedance ratio and Θ is the maximum impedance angle to the positive X direction (Fig. 3, *c*).

We also investigated MV responses obtained from the ratio of the horizontal and vertical magnetic field components. Figure 2, *d* shows a frequency-domain N_{mv} cross section showing high lateral heterogeneity ($\delta \gg 0.05$), with the lowest tippers in the sedimentary craton cover and relatively conductive zones, and the highest tippers in highly-resistive rocks and within the intracrustal conductor.

According to the available geological and geophysical data, the crust in the northwestern profile flank has quite a simple layered-and-mosaic structure with largely spaced heterogeneities (craton basement). The southeastern flank is strongly heterogeneous, both in the upper and lower crust sections. The upper crust behaves mainly in a 2D way while the lower crust bears signature of deep-seated processes of different ages, including those related to rifting, which produced an intricate distribution of material at different depths. Inasmuch as MT data have been collected on a single line, we have to confine ourselves to two dimensions and consider the whole section as an NE structure including the following elements:

(1) shallow subsurface corresponding to 2.5–3 km thick sediment cover;

(2) resistive upper crust (700–1000 ohm · m) with conductive features at different depths and of different conductivities;

(3) nearly vertical conductors corresponding to large faults;

(4) high-resistivity zones corresponding to exposed metamorphic basement (Amga uplift) in the northwestern flank of the profile and to various plutonic and high-grade collisional complexes in the southeast.

There are several depth intervals in East Siberia where the MT field is distorted (Spichak, 2009), most effects being of galvanic origin. The shallowest one is in the uppermost crust, another is in the so-called subsalt complex, and one more heterogeneous layer occurs in the upper crust. Figure 4 shows longitudinal ($\rho^{\parallel}$) and transverse ($\rho^{\perp}$) apparent resistivity curves for I–I. The $\rho^{\parallel}$ curves have prominent lows that record a conductor at depths 16–20 km (Fig. 4, *a*), while the $\rho^{\perp}$ curves are shifted upward on the resistivity axis; the more resistive the anomalies in the upper and middle crust, the greater the shift (Fig. 4, *b*). In this case, deep crust can be resolved only with the use of "quasi-longitudinal" curves (Berdichevsky and Dmitriev, 2009) chosen following a special interactive procedure incorporated into *LineInterMT* software for in-line MT data.

The modeling results have checked by fitting to measured $\rho^{\parallel}$ curves and to the global MV curve (Fig. 3, *d*). The computed curves represent responses of a "normal" gradient-layered earth in regions of different thermodynamic conditions and provide geographic and petrological constraints on the

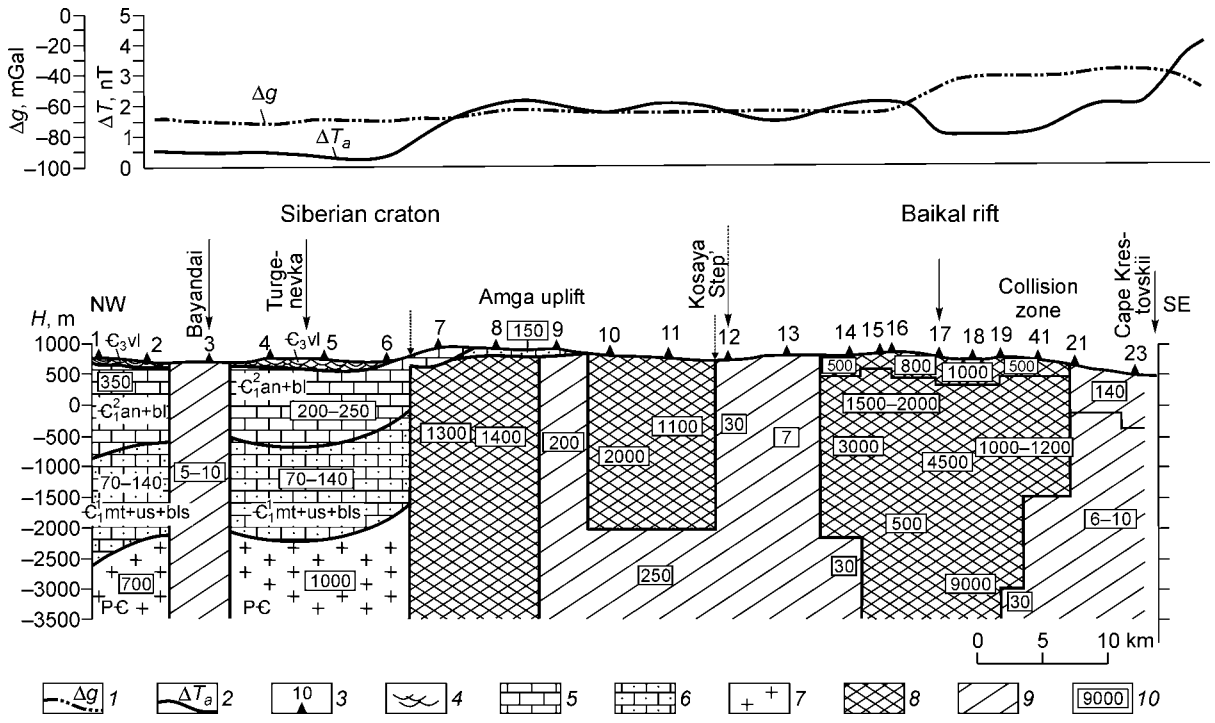

Fig. 6. Resistivity structure of upper crust along profile I–I. *1*, gravity field Δ*g*; *2*, magnetic field ΔT_a; *3*, MT stations; *4*, mainly terrigenous sediments; *5*, limestone; *6*, sandy limestone; *7*, granitic basement (granite and migmatite); *8*, high-resistivity zones (metamorphic complexes of granite gneiss, granite, and ultramafic rocks); *9*, high-resistivity zones; *10*, MT resistivities.

resistivity features distinguished by MT surveys (Pospeyev, 1989). The measured $\rho^{\parallel}$ curves, in their resistivity and depth of the crustal conductor, correspond to the standard curves for rift zones, while their right-hand branches fit the MV curve at $T > 100$ s (Fig. 3, *d*).

Further processing work of the obtained ID inversion results includes corrections for the skin effect (*S*) and preparing the data for final modeling.

Geological interpretation of MT data

The resistivity patterns are different in the northwestern and southeastern parts of the profile (Figs. 5, 6).

The ***northwestern*** profile segment runs across the craton-rift junction exposed to major influence from the rifting activity (Fig. 7). According to Logachev (2007), "the effects of rifting are traceable in Danian–Maastrichtian deposits in "young" synclinal basins in the southeastern craton margin. Although the pebble, sand, and clay that fill the basins are rather thin (within 20–30 m) and occur 70 km away from the Baikal rift basin, their proximity and conformity to the latter prompt that the subsidence and the resulting shallow basins must be anyhow related with the onset of rift opening and must record the earliest activity pulse." The Late Cretaceous basins are controlled by large NE faults and are marked by weak Bouguer gravity lows of the same strike. The resistivities in this area are as high as 500 to 2000 ohm · m or higher.

The craton area covered by the MT surveys includes two metamorphic complexes (Vitte, 1981). Namely, the lower crust consists of granulite-facies hypersthene-magnetite and hypersthene-biotite gneisses, two-pyroxene schists, marble and calciphyre. The metamorphic rocks coexist with numerous concordantly lying charnockite intrusions (lower-crust granitoids) which emplaced with segregation of magnetite and thus

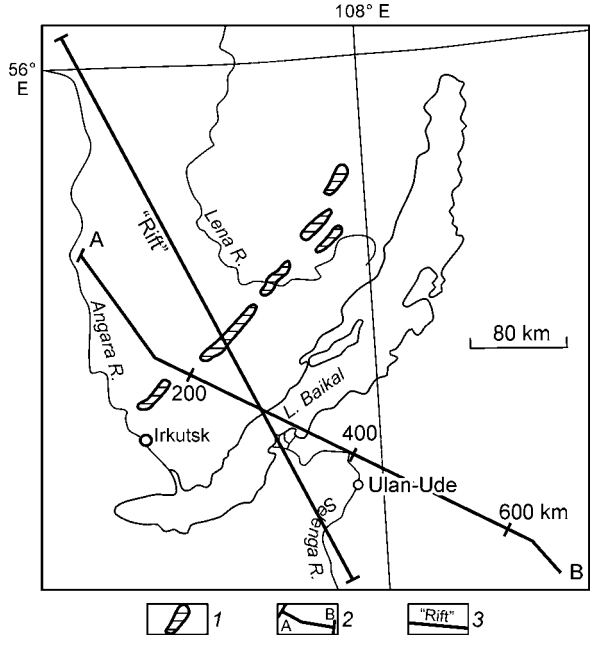

Fig. 7. Cretaceous–Paleocene deposits in Baikal area and in western Transbaikalia (Logachev, 2007). *1*, Danian–Maastrichtian deposits in basins; *2*, DSS profile Ust'-Uda–Lake Baikal–Khilok (Mishen'kin et al., 1999); *3*, Rift transect (Egorkin et al., 1996).

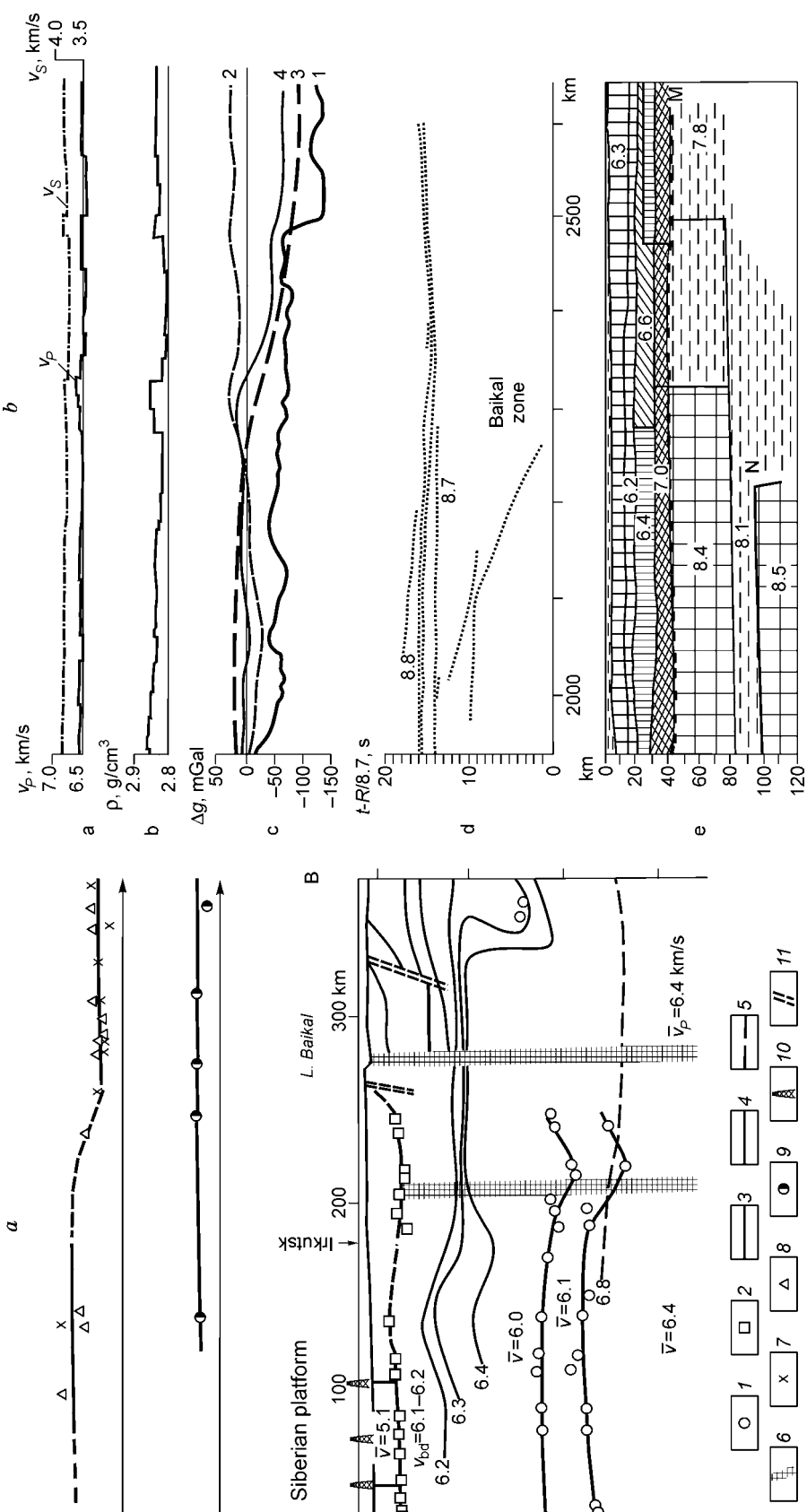

Fig. 8. Crust and upper mantle structure, from seismic profiling data. *a*: DSS profile Ust'-Uda–Lake Baikal–Khilok (Mishenkin et al., 1999). *1, 2*, depths according to reflected and refracted wave data; *3*, seismic interfaces; *4*, velocity contour lines (km/s); *5*, the same, from nonchecked evidence; *6*, large faults; *7* and *8*, Moho boundary velocities (v_{bd}), from refracted waves and from jointly processed reflection and refraction profiling data, respectively; *9*, average crustal velocities, from reflection data; *10*, boreholes; *11*, shallow faults. *b*: *Rift* transect (Egorkin et al., 1996). (a) average *P*- and *S*-wave velocities in consolidated crust; (b) average density of consolidated crust calculated from $\rho = f(v_P, v_S)$ (Krylov, 1993); (c) measured (curve 1) and even (curves 2–4) Bouguer gravity anomalies: curve 2 is effect of crustal structures, curve 3 is effect of upper mantle structures, curve 4 is total model field; (d) measured mantle traveltime curves normalized to 8.7 km/s; (e) seismic cross section of crust and upper mantle. For location of profiles see Fig. 6.

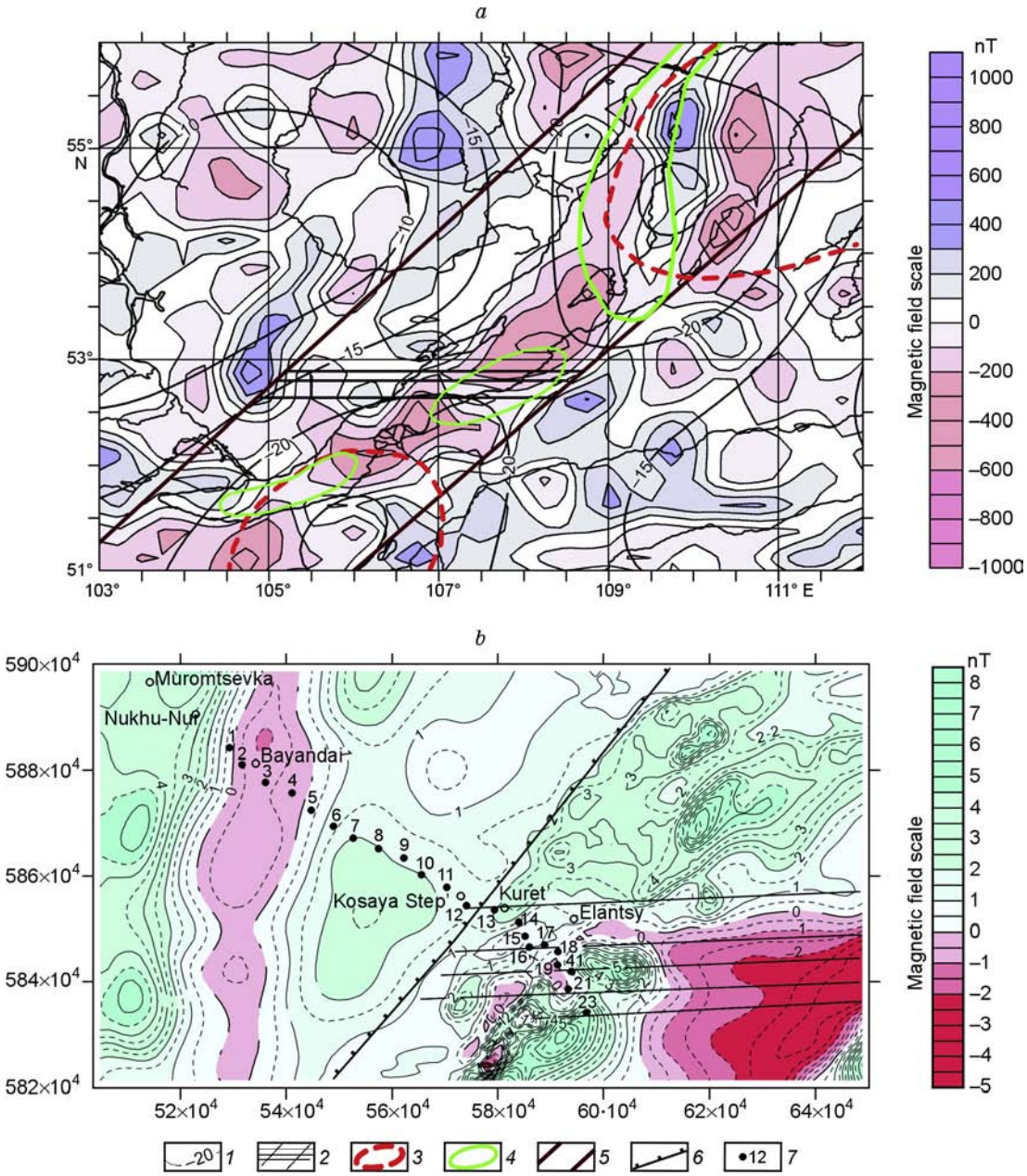

Fig. 9. *a*: Map model of lithospheric magnetic field NGDC-720, harmonics 16-720; *b*: map of anomalous magnetic field T_a: *1*, contour lines of average isostatic anomalies; *2*, large rift-related faults; *3*, horizontal sections of plume tails (Zorin and Turutanov, 2005); *4*, zones of high heat flow (Lysak and Zorin, 1976); *5*, boundaries of Baikal rift; *6*, boundary of remobilized craton, including Ol'khon collision zone; *7*, MT stations.

magnetized the granulites (>2100×10^{-6} CGSM). The rocks of the complex have high density (2.79–2.99 g/cm^3) and resistivity (1500–3500 ohm · m or more) (Dortman, 1964). The upper consolidated crust is composed of an amphibolite-facies complex produced by Early Proterozoic high-temperature retrograde metamorphism and plutonism. The metamorphics are concordant with widespread biotite and biotite-hornblende granite gneiss and granitic rocks. The crust density (σ_{av} = 2.76 g/cm^3 (Vitte, 1981)) and magnetization are lower than in the lower complex but the resistivity is higher (1.5×10^8; 2.9×10^8 ohm · m (Dortman, 1964)).

The background Bouguer gravity is quite low (–60 to –70 mGal) and the magnetic anomalies are weak (1.5–2.0×10^{-4} T). Seismic profiles (Fig. 8, *a*, *b*) show increasing *P*- and *S*-wave velocities in the upper crust (above 20 km), from 5.5 to 6.4 km/s and from 3.2 to 3.7 km/s, respectively (Egorkin et al., 1996; Mishenkin et al., 1999). The interval corresponds to amphibolite-facies rocks intruded by biotite- and biotite-hornblende granite and granite gneiss, the gneiss component increasing with depth. This crust composition is responsible for the magnetic field and the low Bouguer gravity, as well as for the resistivity highs.

Large and deep resistivity highs appear between sites 6 and 11, in the area of the Amga basement uplift (Pavlovsky, 1960; Zamaraev, 1967). The uplift, with its apex between stations 6 and 9, is made up mostly of resistive amphibolite-facies rocks,

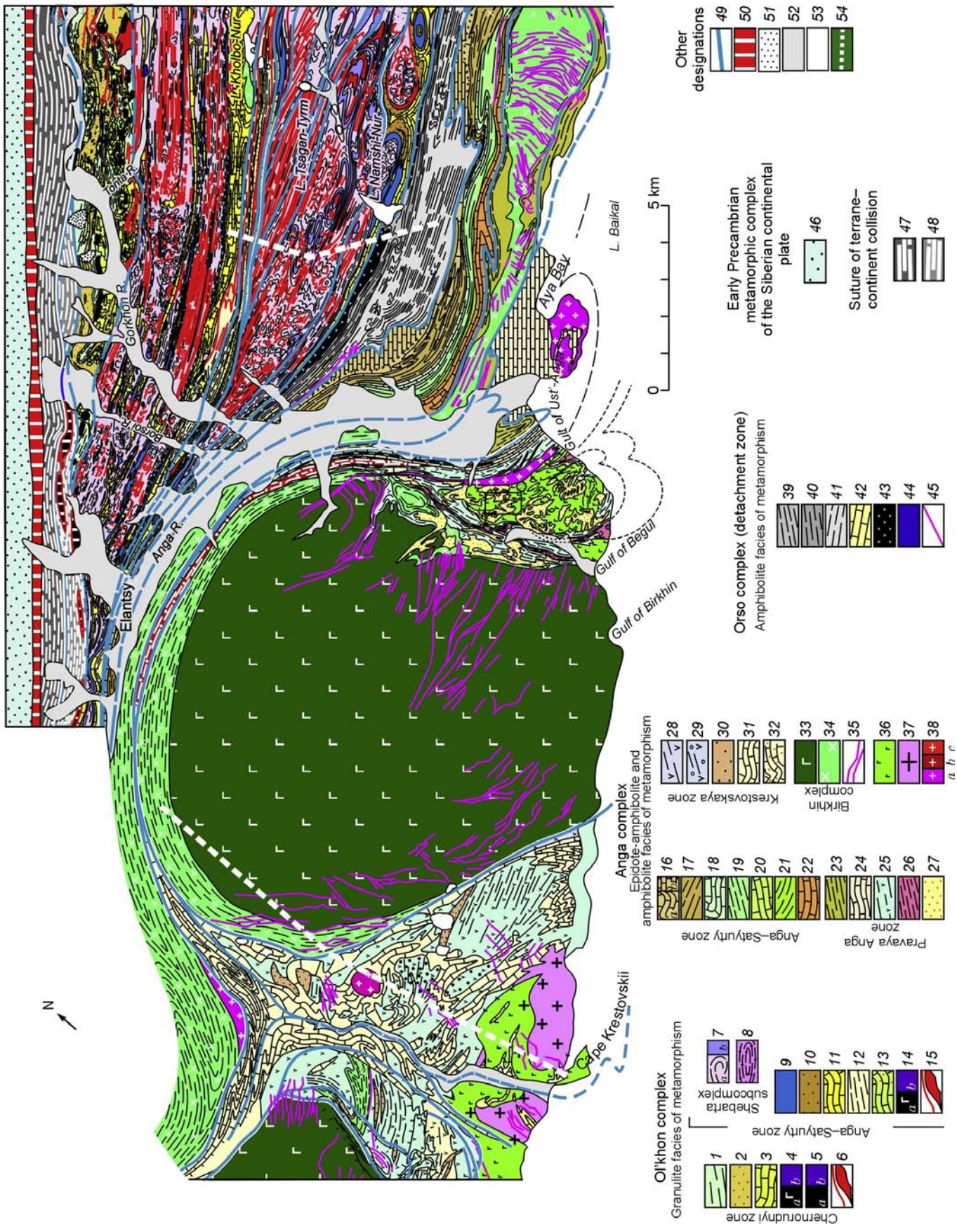
Other designations
49
50
51
52
53
54
Early Precambrian metamorphic complex of the Siberian continental plate
46
Suture of terrane–continent collision
47
48
Orso complex (detachment zone)
Amphibolite facies of metamorphism
39
40
41
42
43
44
45
Anga complex
Epidote-amphibolite and amphibolite facies of metamorphism
Krestovskaya zone
Birkhin complex
Anga–Satyurty zone
Pravaya Anga zone
Ol'khon complex
Granulite facies of metamorphism
Shebarta subcomplex
Anga–Satyurty zone
Chernorudnyi zone
5 km
0
N
L. Baikal
Aya Bay
Gulf of Ust'-Anga
Gulf of Begul'
Gulf of Birkhin
Cape Krestovskii
Elantsy
Anga R.
Bol'shaya R.
Gorkhon R.
Tonta R.
L. Khoibo-Nur
L. Tsagan-Tyrm
L. Namshi-Nur

Fig. 10. Geological map of southwestern Olkhon area, a fragment (Fedorovsky, 2005). Early Paleozoic metamorphic complexes of Olkhon terrane: *1*, two-pyroxene and amphibole-pyroxene schists and gneiss; *2*, quartzite; *3*, marble with forsterite, synmetamorphic marble mélange; *4*, metamorphosed gabbro (*a*) and ultramafic (*b*) rocks within ring intrusions; *5*, metamorphosed gabbro (*a*) and ultramafic (*b*) rocks within mingling dikes; *6*, synmetamorphic vein granite and syenite; *7*, biotite and garnet-biotite gneiss and migmatite (*a*) and amphibolite layers (*b*), traces of Paleoproterozoic protolith (remobilized basement?); *8*, granite gneiss; *9*, amphibolite; *10*, quartzite; *11*, marble and marble mélange-1; *12*, silicate-carbonate gneiss, quartzite; *11*, marble and marble mélange-2; *14*, metamorphosed gabbro (*a*) and ultramafic (*b*) rocks; *15*, synmetamorphic vein granite; *16*, marble-3 (*a*), same marble in zones of transgression (extruded allochthones) (*b*); *17*, amphibolite, silicate-carbonate gneiss; *18*, marble-4; *19* –silicate-carbonate gneiss, amphibolite; *20*, marble-5; *21*, amphibolite; *22*, marble-6; *23*, biotite and garnet-biotite gneiss; *24*, marble-7; *25*, laminated amphibolite; *26*, garnet-andalusite and garnet staurolite schists; *27*, marble mélange of Pravaya Anga zone; *28*, metamorphosed intermediate and mafic volcanics; *29*, metamorphosed brecciated lavas; *30*, quartzite; *31*, marble, sometimes marble mélange in zones of transgression; *32*, marble mélange; *33*, metamorphosed subalkaline gabbro and monzogabbro; *34*, metamorphosed monzodiorite and diorite; *35*, vein granites; *36*, metamorphosed gabbro, Begul complex; *37*, granites (Krestovaya River mouth); *38*, post-metamorphic alkaline granites (*a*), alkaline syenite (*b*), syenite (*c*); *39*, amphibolite, quartzite, microgneiss and related blastomylonite; *40*, tectonic layering of microgneiss and amphibolite. Blastomylonites: *41*, garnet-two-mica microgneiss and related blastomylonite; *42*, marble and marble mélange; *43*, metamorphosed gabbro and gabbro-amphibolite; *44*, metamorphosed ultramafic rocks and related talc schist; *45*, synmetamorphic vein granite; *46*, metamorphosed sandstone and volcanics of Sarma Group. Granites: *47*, blastomylonitic Early Precambrian metamorphics; *48*, blastomylonitic Early Paleozoic metamorphics (*a*), granulite blocks in blastomylonite matrix (melange) (*b*); *49*, synmetamorphic blastomylonite shear zones and thrusts; *50*, present zone of Primorsky Fault in the Baikal rift system; *51*, Cenozoic watershed pebbles; *52*, Quaternary sediments; *53*, structural elements in metamorphic rocks; *54*, a fragment of southwestern profile I–I and profile II–II.

granite gneiss, and granite (see the cross section along I–I in Figs. 5, 6). The resistivities at the uplift center remain high till 25–30 km but decrease below these depths. The same composition and geophysical patterns are at sites 4, 5, 6, and 9.

The zone of abrupt velocity change in the lower section (Fig. 8, *b*), with high average (6.4 km/s) and layer (6.6; 6.9; 7.0 km/s) *P* velocities, may correspond to granulites (Egorkin et al., 1996). The resistivity averaged over this depth interval (15–20 to 30 km) is quite low though the rocks are resistive. The reason is in the presence of a conductor in the crust at 16–20 km, with a resistivity as low as <50 ohm · m, which shows up in $\rho^{\parallel}$ curves at periods 64–144 s (Fig. 4, *a*). The electric parameters and the depth of the conductive layer are controlled by the present thermal regime in the area: the more active the lithosphere the shallower and the less resistive the conductor (Pospeyev, 1976; Pospeyev et al., 1989). It rises to 12–16 km beneath the Baikal rift but is poorly pronounced in the rift center.

The ***southeastern*** part of the profile fully belongs to the Baikal rift zone which lies upon the craton edge and upon the Paleozoic collision suture (Fig. 5). The crust is mostly low resistive (100–50 to 10 ohm · m or less). The subsurface boundary between the two major resistivity units runs near MT station 11, where the pattern changes (Figs. 5, 6). In the upper section it is shifted toward stations 12 and 13. The southeastern unit at stations 11 through 14 is marked by a large resistivity low (from 25 to 5 ohm · m). The conductor is broad to a depth of 20 km, then it narrows down and is traceable to 30 km with slightly higher resistivities (from 50 to 100 ohm · m). Below 20 km the low-resistivity zone is flanked by vertical zones of higher resistivity (to 500 ohm · m).

The profile part between stations 14 and 41 is a high-resistivity zone, with highs especially prominent in the upper section above 6–7.5 km (Figs. 5, 6). The mid-crustal high-resistivity zone of 1500, 4500, and up to 9000 ohm · m at sites 17, 18 spreads to a depth of 20 km, with a fall to 500 ohm · m, where it joins the lower-crust zone (20–30 km) of the same high resistivity. The upper crustal resistivity maximum (850, 1200 ohm · m) located between stations 19 and 41 covers depths over 5 km. At stations 14, 15, and 16 there are high-resistivity features (1500, 2000, 3100 ohm · m) with their bottoms at 1200, 1500, and 2200 m below the surface, while the resistivity decreases to 400 ohm · m at 1500–4500 m beneath stations 15 and 16.

Southeast of station 41, which falls in the resistivity gradient zone, there is a large low of 6–10 ohm · m spreading down to 10 km, while the layer below it (to 30 km) is less conductive (100–200 ohm · m). This block of the crust is bounded by a large vertical fault in the southeast and borders a zone of low resistivity (10 ohm · m or less) in the northwest; northwest of the site there is a mosaic of high- and low-resistivity zones at depths between 15 and 30 km (Fig. 5).

The reported resistivity pattern in the southeastern flank of the MT profile represents a collage of blocks comprising the Olkhon collisional zone as far as the continent-terrane suture (Sklyarov et al., 2001) (Fig. 5) and the exposed basement fragments nearby which were deformed in the course of Paleozoic and Neoproterozoic processes associated with large-scale rifting along the craton margin and intrusion of gabbro-dolerite dikes into the rifted crust (Gladkochub et al., 2005).

The whole collage stands out against the surrounding areas of the Siberian craton as an NE belt of intense magnetic anomalies (Fig. 9, *b*), relative gravity highs, and a shallow high-velocity zone (Fig. 8). The rise of the 6.4 km/s velocity line to 10 km (Fig. 8, *a*) in the seismic cross section along the Ust-Uda–Lake Baikal–Khilok profile (Mishenkin et al., 1999) is evidence of high-density crust below that boundary. Seismic interfaces above and below 20 km rise toward Lake Baikal; the Moho becomes deeper (i.e., the crust thickens up) toward the collision zone.

The Early Paleozoic Olkhon collisional system consists of diverse igneous and metamorphic rocks formed in two main events of terrane–island arc and terrane–continent collisions. The collisional high-temperature metamorphic complex experienced folding, thrusting, and listric and strike-slip faulting and syntectonic plutonism (Sklyarov and Fedorovsky, 2006). There are abundant igneous and metamorphic mingling dikes within the collision zone. As explained in (Sklyarov and Fedorovsky, 2006), magmatic mingling, or mechanic mixing of compositionally different magmas, occurs when mafic magma is injected into a chamber with synmetamorphic

granite magma; the tectonic position of mingling dikes is controlled by strike-slip faulting. At the peak of collisional compression and related faulting, the thick crust collapses and mantle material becomes drained into the middle and upper crust (Sklyarov and Fedorovsky, 2006). Metamorphic mingling results from intrusion of magma into low-viscosity plastic medium (rheologically similar to a granite melt). Once got into the low-viscosity environment involved in tectonic flow, the hot mantle material forms drop-shaped or spherical nodules and rolls into the matrix which experiences synmetamorphic folding (Sklyarov and Fedorovsky, 2006; Sklyarov et al., 2001). The intricate pattern produced by the mingling processes is evident in Fig. 10.

Thus, the crust in the collision zone consists of mafic, ultramafic, and felsic intrusives and granulite-, amphibolite-, and epidote-amphibolite metamorphic rocks.

These rocks are resistive even at rather high temperatures (Lebedev and Khitarov, 1979). Resistivity is fairly high, from 500 to 9000 ohm · m, in the upper 10–15 km of the crust in the central part of the collision zone (stations 17, 18, and 19, Fig. 4). Site 17 covers the suture between the Olkhon system (blastomylonitic Early Precambrian and Early Paleozoic metamorphic complexes with large ultramafic blocks embedded in the blastomylonite matrix) and marble mélange in the south that encloses large and small metamorphosed ultramafic bodies (Fig. 10).

The resistivity high between stations 17 and 18 marks aligned granite gneiss domes in amphibolite-facies rocks (Dortman, 1976) which are recognizable to depths of 20 km, with the resistivity decreasing depthward to 200–300 ohm · m at the boundary with a large low-resistivity zone. The high beneath stations 19 and 41 corresponds to metamorphosed subalkaline gabbro and monzogabbro in the Oval dome and its amphibolite-gneiss fringe (Fig. 10). The 850–1200 ohm · m feature spreads to 3 km (station 19) and borders a low-resistivity zone below that depth at station 41 (Fig. 10).

High-resistivity (1500–3100 ohm · m) responses measured in the upper crust at sites 14, 15, and 16 (Fig. 5) are from granitoids. At depths 6–7 km beneath the plutons, the resistivity decreases to 100 and 50 ohm · m being part of a large low-resistivity zone (sites 11, 12, and 13). The depth interval from 20 to 30 km beneath stations 14, 15, and 16, as well as 11 and 12, includes zones of relatively high resistivity, which most likely correspond to basaltic and granitic intrusions according to the history of the collision zone (see above). They are separated from the high-resistivity zones in the upper crust by local lows that obscure the links between resistive features throughout the collision zone.

Geological interpretation of resistivity lows

It is pertinent to begin the discussion on the origin of resistivity lows with a synopsis of the earlier experience.

1. Magnetotelluric soundings in the Baikal rift furnish independent evidence of the thermal and fluid regimes in the lithosphere (Baryshev et al., 1989; Gornostaev et al., 1970; Pospeyev and Van'yan, 1978; Pospeyev et al., 1978, 1996). MT data can be integrated with seismic data to correlate conductive layers in the crust with seismic waveguides (Krylov et al., 1993; Puzyrev, 1981; Song et al., 1996).

2. Currently, conductive crust in the Baikal rift (Kiselev and Popov, 2000; Pospeyev, 1996) is most often attributed to the effect of aqueous fluids presumably coming from the upper mantle. This hypothesis provides the least controversial explanation for fluidization in the middle crust of the area and for many problematic issues of geology and geophysics. It agrees with the idea that rifted crust is especially favorable for discharge of mantle fluids.

The thermal regime in the Baikal rift involves conductive and convective heat transport, the latter being associated with fluids and being commensurate with conductive heat flow (Golubev, 2007). The resistivity patterns with large lows in the middle and lower crust can be interpreted with reference to ideas of how heat flow anomalies form in the Baikal rift (Golubev, 2007):

– the rifted lithosphere is highly permeable, and the permeable zones (large faults) can vent mantle fluids;

– high conductive heat flow observed in the rift is largely due to advective heat transport by mantle fluids;

– upper mantle in the area does contain abundant fluids that rise to the surface along permeable zones and are continuously recharged from deeper fluids;

– the model of mixed conductive and convective heat transport implies heat recharge of thermal anomalies in the rift without changes in crust composition beneath the anomalies.

Thus, the crust in the area of MT surveys, especially within the collision zone, is heavily faulted and the faults vent mantle fluids which, in turn, constantly feed from fluids deeper in the mantle. The convective heat carried by fluids, together with conductive heat, makes the crust warmer and less resistive.

The large resistivity lows in the collision zone (stations 11–14 and 18–23) can be explained with reference to the deep structure and heat flow patterns in the rift. Figure 9, *a* shows magnetic anomalies (an averaged model of lithospheric magnetic field NGDS-720) and isostatic gravity anomalies averaged over a radius of 200 km that record the mantle density (Artem'ev, 1966). Northern Lake Baikal and the adjacent part of Transabikalia in the east fall into a gravity low (–25 mGal). The contours of the low fit the horizontal section of a plume tail (Zorin and Turutanov, 2005); the same zone is marked by a heat flow high of > 90 mW/m^2 (Balobaev et al., 1985). Another negative isostatic gravity anomaly (–25 mGal) appears in southern Baikal and Transbaikalia next to it and corresponds to shallow-lying low-density mantle (a plume) and to a heat flow high. The plumes are separated by several W–E faults that laterally confine the rifted crust. According to geophysical evidence, they do not transcend the master faults (Fig. 9, *a*) that border the rift system. The large W–E faults are expressed in magnetic anomalies measured by land surveys (Fig. 9, *b*). The tectonic position of these faults implies active discharge of mantle fluids. Given that stations 12, 13, 14, 15, 16, 17, 18, 19, 21, 23, and 41 of the profile cover the faulted zone, the hypothesized constant recharge of

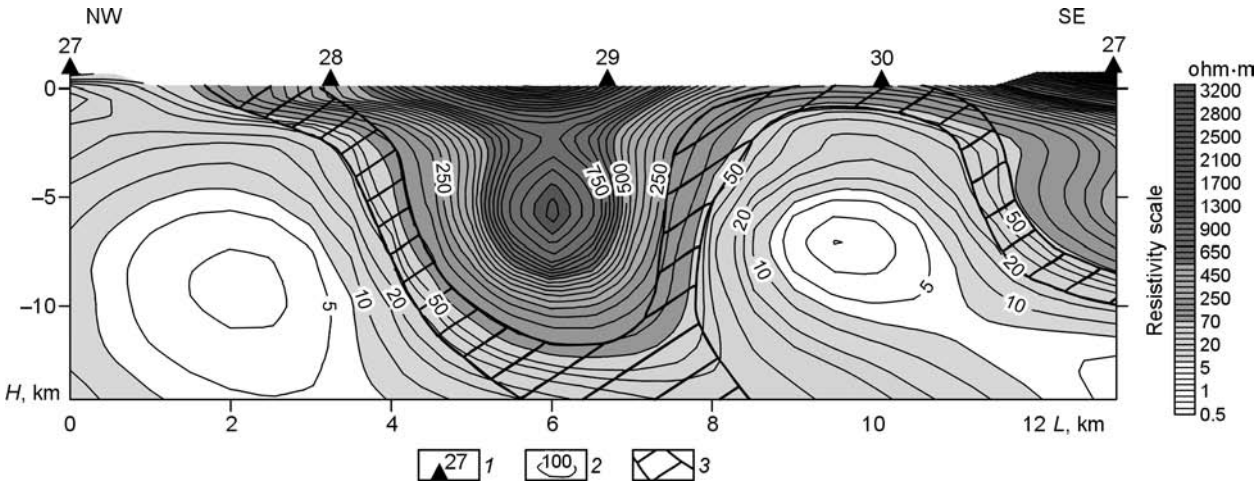

Fig. 11. Deep resistivity cross section along profile II–II. *1*, MT stations; *2*, resistivity contour lines (ohm · m); *3*, blastomylonitic gneiss, amphibolite, and other rocks.

the fluids from deeper mantle may account for the large resistivity lows.

Stations 41 and 19 are located within the Oval dome (Fig. 10) composed of resistive metamorphosed subalkaline gabbro and monzogabbro, silicate-carbonate gneiss, and amphibolite (Dortman, 1976). However, relatively high resistivity (of 1200 ohm · m) has been measured only at site 41. The same is the setting of stations 21 and 23 where resistivities as low as 6–10 ohm · m fall into granitoids known to be resistive at normal *PT* conditions; low resistivities (5, 10, 25 ohm · m) appear also in the lower section beneath stations 18, 19, and 41, respectively. All these resistivity lows may be due to fluids venting through large W–E faults.

A large resistivity low bounded by vertical rift faults at sites 11, 12, 13, and 14 spreads to about 20 km beneath station 12 and to 30 km beneath 13 (Fig. 5). These stations are located within a W–E rift border fault while site 13, according to geophysical evidence, falls into an NE large fault that bounds the whole collision system (Fig. 9, *a*). This may be the reason why the resistivity low is so deep there.

Profile II–II is restricted to the collision zone, from the suture (terrane–continent) and almost as far as the Baikal shore (between stations 27 and 31). The section images only the upper crust with different resistivities. The resistivity pattern highlights the tectonic activity in the collision zone: a dense network of faults that bound shear zones with blastomylonite sutures between them (Sklyarov et al., 2001). There are zones of thrusting, doming, and strike-slip faulting. A dome occurs beneath MT stations 28 and 29 and is composed of biotite and garnet-biotite gneiss and migmatite enclosing amphibolite layers. This structure, with abundant granite gneiss domes, represents remobilized basement (Sklyarov et al., 2001). In the northwest and southeast, there are thick zones of blastomylonitic gneiss, amphibolite, and quartzite. The MT image clearly shows the thrust and strike-slip geometry of faulting at the boundaries between compositionally different zones (Fig. 11).

Conclusions

The resistivity structure in the area imaged by magnetotelluric soundings and correlated with other geological and geophysical data is generally as follows:

1. The crust comprises two major resistivity units: the northwestern and southeastern flanks of the profile corresponding, respectively, to the transition from the Siberian craton to the Baikal rift and to the rift zone itself.

2. The northwestern profile flank is highly resistive due to high-grade metamorphic and granitic crust of the craton basement. It is partly covered with sediments which include three resistivity layers pinching out toward the basement uplift. There is a conductor with its top resolved at depths about 16–20 km indicating ongoing activity. The conductive layer is superposed with nearly vertical conductive features that reach the upper crust and may result from fluids rising from the mantle through the permeable rifted crust.

2. The crust in the southeastern profile part contains two large conductors that spread down from the uppermost crust to a depth of 30 km and are separated by a mosaic of high-resistivity zones corresponding to resistive rocks in the collision zone. This profile segment is heavily faulted, and the faults vent mantle fluids which heat up the crust and make it less resistive.

References

Adam, A., 1976. Quantitative connections between regional heat flow and the depth of conductive layers in the Earth's crust and upper mantle. Acta Geodaetica, Geophysica et Montanistica (Acad. Sci. Hungary) 11, 503–509.

Artem'ev, M.E., 1966. Isostatic Gravity Anomalies and Some Interpretation Issues [in Russian]. Nauka, Moscow.

Bahr, K., 1988. Interpretation of magnetotelluric impedance tensor: regional induction and local telluric distortion. J. Geophys. 62, 119–127.

Balobaev, V.T. (Ed.), 1985. Catalog of Heat Flow Data from Siberia (1966–1984) [in Russian]. IGiG SO AN SSSR, Novosibirsk.

Baryshev, A.S., Pospeyev, V.I., Nikulin, V.I., Ipat'ev, S.N., Mandelbaum, M.M., Pis'mennyi, B.M., Alakshin, A.M., 1989. Deep structure of

the Baikal fold area and its junction with the Siberian craton, in: Proc. 28th IGC, Deep Geophysical Soundings in the USSR. Nauka, Moscow, pp. 163–173.

Berdichevsky, M.N., Dmitriev, V.I., 2009. Magnetotelluric Surveys: Models and Methods [in Russian]. Nauchnyi Mir, Moscow.

Berdichevsky, M.N., Dmitriev, V.I., Novikov, D.B., Pastutsan, V.V., 1997. Processing and Interpretation of MT Data [in Russian], Dialog MGU, Moscow.

Berdichevsky, M.N., Van'yan, L.L., Koshurnikov, A.V., 1999. Magnetotelluric surveys in the Baikal rift, Izv. RAN, Fizika Zemli, No. 10, 17–35.

Dortman, N.B. (Ed.), 1964. Physical properties of Rocks and Minerals in the USSR [in Russian]. Nedra, Moscow.

Dortman, N.B. (Ed.), 1976. Physical properties of Rocks and Minerals. A Handbook [in Russian]. Nedra, Moscow.

Egorkin, A.V., Pavlenkova, N.I., Romanyuk, T.V., Solodilov, L.N., 1996. The upper mantle structure along the "*Rift*" Baikal–Yamal profile according to data of an exploring nuclear explosion. Geologiya i Geofizika (Russian Geology and Geophysics) 37 (9), 66–76 (66–74).

Gladkochub, D.P., Donskaya, T.V., Mazukabzov, A.M., Sklyarov, E.V., Stanevich, A.N., 2005. Neoproterozoic evolution of the southern Siberian craton: Petrology and geochronology of igneous complexes and their possible links with Rodinia breakup and Paleoasian ocean opening, in: Leonov, M. (Ed.), Problems of Central Asian Tectonics [in Russian]. GEOS, Moscow, pp. 127–136.

Golubev, V.A., 2007. Conductive and Convective Heat Transport in the Baikal Rift [in Russian]. Akademicheskoe Izd. "Geo", Novosibirsk.

Gornostaev, V.P., 1967. Some additional evidence of deep structure in the Baikal region (from resistivity survey data). Geologiya i Geofizika, No. 11, 98–103.

Gornostaev, V.P., 1979. Magnetotelluric Soundings in the Lake Baikal basin. Izv. AN SSSR, Fizika Zemli, No. 6, 99–101.

Gornostaev, V.P., Mikhalevsky, V.I., Pospeyev, V.I., 1970. Deep magnetotelluric soudings in the southern Siberian craton and in the Baikal rift zone. Geologiya i Geofizika, No. 4, 111–117.

Kiselev, A.I., Popov, A.M., 2000. The Baikal rift as a portrayal of dynamic, structural, and compositional differences between the lithosphere of the Siberian craton and the Central Asian Mobile Belt. Dokl. Earth Sci. 371 (2), 226–229.

Krylov, S.V. (Ed.), 1993. Detailed *P*- and *S*-wave Soundings of the Lithosphere [in Russian]. Nauka, Novosibirsk.

Lebedev, E.B., Khitarov, N.I., 1979. Physical Properties of Magma Melts [in Russian]. Nauka, Moscow.

Letnikov, F.A., Karpov, I.K., Lashkevich, V.V., 1977. Machine-aided modeling of the multiple system Fe2O3–Fe3O4–O2–H2 at 200–1000 °C and 1–10,000 bar, in: Fluid Regime in Crust and Upper Mantle [in Russian]. Nauka, Novosibirsk, pp. 33–34.

Logachev, N.A., 2007. History and geodynamics of the Baikal rift, in: Sherman, S.I., Levi, K.G., Dorofeeva, G.P. (Eds.), Nikolai Alekseevich Logachev [in Russian], Izd. SO RAN, Novosibirsk, pp. 194–226.

Lysak, S.V., Zorin, Yu.A., 1976. The Thermal Field of the Baikal Rift and its Surroundings [in Russian]. Nauka, Moscow.

Mishenkin, B.P., Mishenkina, Z.R., Petrik, G.V., Sheludko, I.F., Mandelbaum, M.M., Seleznev, V.S., Soloviev, V.M., 1999. DSS studies of the crust and upper mantle in the Baikal rift. Izv. RAN, Fizika Zemli, No. 7–8, 74–93.

Pavlovsky, E.V., 1960. The Late Precambrian (Upper Proterozoic) of the Western and Eastern Baikal region, in: Proc. 21st IGC, Stratigraphy and Correlation of the Precambrian, Izd. AN SSSR, Moscow, pp. 131–135.

Popov, A.M., 1990. A deep geophysical study in the Baikal region. PAGEOPH 134 (4), 575–587.

Pospeyev, V.I., 1976. Deep magnetotelluric surveys of the Siberian platform and the Baikal rift zone, in: Adam, A. (Ed.), Geoelectric and Geothermal Studies. Academia Kiado, Budapest, pp. 673–681.

Pospeyev, A.V., 1996. Geophysical evidence of fluids in the crust, in: Geophysical Studies in East Siberia at the Turn of the Century [in Russian]. Nauka, Novosibirsk, pp. 38–42.

Pospeyev, V.I., Van'yan, L.L., Gornostaev, V.P., 1978. Deep resistivity structure of the Baikal and Pacific rift zones, in: Proc. All-Union Seminar on Resistivity Surveys [in Russian]. Moscow University Press, Moscow, pp. 45–51.

Puzyrev, N.N. (Ed.), 1981. Interior of Baikal, from Seismic Data [in Russian]. Nauka, Novosibirsk.

Sklyarov, E.V., Fedorovsky, V.S., 2006. Magma mingling: Tectonic and geodynamic aspects. Geotektonika, No. 2, 47–64.

Sklyarov, E.V., Fedorovsky, V.S., Gladkochub, D.P., Vladimirov, A.G., 2001. Synmetamorphic basic dikes as indicators of collision structure collapse in the western Baikal region. Dokl. Earth Sci. 381A (9), 1028–1033.

Song, Youngsheng, Krylov, S.V., Yang, Baojun, Liu, Cai, Dong, Shixue, Liang, Tiechen, Li, Jingzhi, Xu, Xingzui, Mishen'kina, Z.R., Petrik, G.V., Shelud'ko, I.F., Seleznev, V.S., Sokolov, V.M., 1996. Deep seismic sounding of the lithosphere on the Baikal–Northeastern China International Transect. Geologiya i Geofizika (Russian Geology and Geophysics) 37 (2), 3–15 (1–13).

Spichak, V.V. (Ed.), 2009. Electromagnetic Data: Advanced Methods of Acquisition, Processing, and Interpretation [in Russian]. Librokoma, Moscow.

Swift, C.M., 1967. A Magnetotelluric Investigation of an Electrical Conductivity Anomaly in the Southwestern United States. Dissertation MIT, Cambridge.

Vitte, L.V., 1981. Types of Continental Crust and Their Evolution [in Russian]. Nauka, Novosibirsk.

Zamaraev, S.M., 1967. The Border Structures in the Southern Siberian Craton [in Russian]. Nauka, Moscow.

Zorin, Yu.A., Turutanov, E.Kh., 2005. Plumes and geodynamics of the Baikal rift zone. Russian Geology and Geophysics (Geologiya i Geofizika) 46 (7), 669–682 (685–699).

Editorial responsibility: A.D. Duchkov